THE JOURNAL OF BIOLOGICAL CHEMISTRY VOL. 283, NO. 52, pp. 36617–36623, December 26, 2008

Catalytic Mechanism of Nitrile Hydratase Proposed by Time-resolved X-ray Crystallography Using a Novel Substrate, *tert*-Butylisonitrile*[S]

Received for publication, August 25, 2008, and in revised form, September 26, 2008 Published, JBC Papers in Press, October 23, 2008, DOI 10.1074/jbc.M806577200

Koichi Hashimoto[‡], Hiroyuki Suzuki[§], Kayoko Taniguchi[¶], Takumi Noguchi[§], Masafumi Yohda[‡], and Masafumi Odaka[§1]

From the [‡]Department of Biotechnology and Life Science, Graduate School of Technology, Tokyo University of Agriculture and Technology, 2-24-16 Naka-cho, Koganei, Tokyo 184-8588, Japan, the [§]Institute of Materials Science, University of Tsukuba, Tsukuba 305-8573, and [¶]Eco-Soft Material Research Units, RIKEN, Wako, Saitama 351-0198, Japan

Nitrile hydratases (NHases) have an unusual iron or cobalt catalytic center with two oxidized cysteine ligands, cysteine-sulfinic acid and cysteine-sulfenic acid, catalyzing the hydration of nitriles to amides. Recently, we found that the NHase of *Rhodococcus erythropolis* N771 exhibited an additional catalytic activity, converting *tert*-butylisonitrile (*t*BuNC) to *tert*-butylamine. Taking advantage of the slow reactivity of *t*BuNC and the photoreactivity of nitrosylated NHase, we present the first structural evidence for the catalytic mechanism of NHase with time-resolved x-ray crystallography. By monitoring the reaction with attenuated total reflectance-Fourier transform infrared spectroscopy, the product from the isonitrile carbon was identified as a CO molecule. Crystals of nitrosylated inactive NHase were soaked with *t*BuNC. The catalytic reaction was initiated by photo-induced denitrosylation and stopped by flash cooling. *t*BuNC was first trapped at the hydrophobic pocket above the iron center and then coordinated to the iron ion at 120 min. At 440 min, the electron density of *t*BuNC was significantly altered, and a new electron density was observed near the isonitrile carbon as well as the sulfenate oxygen of αCys^{114}. These results demonstrate that the substrate was coordinated to the iron and then attacked by a solvent molecule activated by αCys^{114}-SOH.

Nitrile hydratases (NHases)[2] catalyze the hydration of nitriles to the corresponding amides and are used as catalysts in the production of acrylamide, making them one of the most important industrial enzymes (1, 2). NHases contain a non-heme Fe^{3+} or non-corrin Co^{3+} catalytic center. Iron-type NHases show unique photoreactivity; the enzyme is inactivated by nitrosylation in the dark and immediately reactivated by photo-induced denitrosylation (3–5). The protein structure is highly conserved among all known NHases (6–9) as well as a related enzyme, thiocyanate hydrolase (10). The metal site is also conserved, with a distorted octahedral geometry. All ligand residues are involved in a strictly conserved motif of the α subunit, Cys^1-Xaa-Leu-Cys^2-Ser-Cys^3, where two amide nitrogens of Ser and Cys^3 and three Cys sulfurs are coordinated to the metal (6). Cys^2 and Cys^3 are post-translationally modified to cysteine-sulfinic acid and cysteine-sulfenic acid, respectively (7), which probably take deprotonated forms at the metal site (11). The sixth ligand site is occupied by a solvent molecule (8) or by a NO molecule in nitrosylated iron-type NHase (7).

Several reaction mechanisms have been proposed based on the protein structures (1, 6). First, nitriles directly bind to the metal to facilitate the nucleophilic attack of a water molecule on the nitrile carbon. In the other mechanisms, a water molecule activated by the metal directly or indirectly attacks nitriles trapped near the metal. In all cases, the metal is suspected to function as a Lewis acid. By reconstituting iron-type NHase from recombinant unmodified subunits, we demonstrated that the post-translational modifications of its cysteine ligands are essential for its catalytic activity (12). We also found that specific oxidation of the cysteine sulfenic acid ligand to cysteine sulfinic acid resulted in irreversible inactivation (13). Kovacs and co-workers (14) studied the ligand exchange reaction in the low spin Co^{3+}-containing NHase model complexes and concluded that the *trans*-thiolate sulfur played an important role in promoting the ligand exchange at the sixth site. Later, by using a sulfenate-ligated iron complex, they showed that protonation/deprotonation states of the sulfenate oxygen were modulated by the unmodified Cys thiolate ligand (15). An N_3S_2-type model complex, $[Co(PyPS)(H_2O)]^-$, slowly hydrolyzes nitriles

* This work was supported in part by a Grant-in-aid for scientific research from the "Future nano materials" section of the "21st Century Center of Excellence" Project, Grant-in-Aid for Scientific Research (B) KAKENHI 19350080 (to M. O.), Grant-in-Aid for Creative Scientific Research 17GS0314 (to T. N.), Grant-in-Aid from the Japanese Society for the Promotion of Science Fellows 19252 (to H. S.), and a grant from the National Project on Protein Structural and Functional Analyses from the Ministry of Education, Science, Sports and Culture of Japan (to M. Y.). The costs of publication of this article were defrayed in part by the payment of page charges. This article must therefore be hereby marked "*advertisement*" in accordance with 18 U.S.C. Section 1734 solely to indicate this fact.

[S] The on-line version of this article (available at http://www.jbc.org) contains supplemental Figs. S1 and S2.

The atomic coordinates and structure factors (code 2ZPB, 2ZPE, 2ZPF, 2ZPG, 2ZPH, and 2ZPI) have been deposited in the Protein Data Bank, Research Collaboratory for Structural Bioinformatics, Rutgers University, New Brunswick, NJ (http://www.rcsb.org/).

[1] To whom correspondence should be addressed: Dept. of Biotechnology and Life Science, Graduate School of Technology, Tokyo University of Agriculture and Technology, 2-24-16 Naka-cho, Koganei, Tokyo 184-8588, Japan. Tel./Fax: 81-42-388-7479; E-mail: modaka@cc.tuat.ac.jp.

[2] The abbreviations used are: NHase, nitrile hydratase; *Re*NHase, nitrile hydratase from *R. erythropolis* N771; *t*BuNC, *tert*-butylisonitrile; *t*BuNH$_2$, *tert*-butylamine; ATR-FTIR, attenuated total reflectance-Fourier transform infrared.

(18 turnovers in 4 h) (16). Interestingly, the hydration activity was enhanced by the mono-oxygenation of one of two sulfur ligands (17). Heinrich *et al.* (18) demonstrated that Na[Co(L-N_2SOSO)(*t*BuNC)$_2$] exhibited the nitrile hydration activity but that (Me_4N)[Co(L-$N_2SO_2SO_2$)(*t*BuNC)$_2$] did not. These results indicate that the oxidized cysteine ligands, especially the cysteine sulfenic acid ligand, play an important role in the catalysis. Recently, theoretical calculations, including density functional calculations (19, 20) as well as molecular dynamics simulations (21), have been applied to the mechanisms described above. However, the detailed mechanism remains unclear because of a lack of direct information on the reaction intermediates.

We recently found that an iron-type NHase from *Rhodococcus erythropolis* N771 (*Re*NHase) catalyzes the conversion of isonitriles to the corresponding amines (22). Although the other product derived from the isonitrile carbon was not identified, the kinetic analyses revealed that the K_m for *t*BuNC was comparable with that for methacrylonitrile, whereas k_{cat} (1.8×10^{-2} s^{-1}) was 1.8×10^5 times smaller. In this study, taking advantage of the slow reactivity of *t*BuNC as well as the photoreactivity of nitrosylated inactive *Re*NHase (3, 4), we obtained structural evidence on the reaction mechanism by studying the time course of the *t*BuNC catalysis with x-ray crystallography. Based on the results, we propose a reaction mechanism in which the sulfenate group of αCys^{114}-SO^- plays a key role in the catalysis.

EXPERIMENTAL PROCEDURES

Materials—Nitrile hydratase from *R. erythropolis* N771 (*Re*NHase) was inactivated by endogenous NO molecules in living cells in the dark (4, 23). *Re*NHase was purified in the nitrosylated form in the dark as described previously (23). The purified nitrosylated *Re*NHase was stored in 50 mM Tris-HCl, pH 7.5, at −80 °C in the dark at a concentration of 20 mg/ml. The concentration of the nitrosylated NHase was determined by measuring the absorbance at 280 nm (ϵ_{280} = 1.7 ml mg^{-1} cm^{-1}). *t*BuNC was purchased from Tokyo Chemical Industry Co., Ltd. (Tokyo, Japan). All the other reagents used in this study were of the highest grade available.

ATR-FTIR Measurements—The nitrosylated *Re*NHase (70 mg/ml) in 50 mM sodium phosphate, pH 7.5, was loaded on the surface of a three-reflection silicon prism (3 mm in diameter) in the ATR accessory (DuraSampl*IR* II, Smiths Detection, Danbury, CT) and dried under nitrogen gas flow. Subsequently, 1.5 μl of water ($H_2{}^{16}O$ or $H_2{}^{18}O$) was added to the sample. The sample space was sealed with a CaF_2 plate and a greased Teflon spacer (0.7 mm in thickness). The substrate, 0.5 μl of neat *t*BuNC, was also enclosed in this sealed space as a drop on the CaF_2 plate, to be supplied to the *Re*NHase solution as a vapor. The sample was stabilized at room temperature in the dark for 4 h.

FTIR spectra were measured on a Bruker IFS-66/S spectrophotometer equipped with an MCT detector (D313-L). All of the spectra were recorded at 4 cm^{-1} resolution. A single-beam spectrum was recorded for 100 s before illumination, and ten spectra (100 s scans) were successively recorded after 10 s of illumination by continuous white light from a halogen lamp (Hoya-Schott HL150; ~60 milliwatt cm^{-2} at the sample).

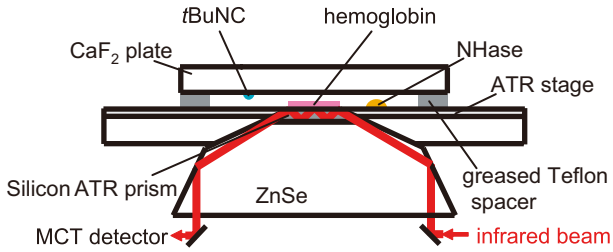

FIGURE 1. **The sample unit of the ATR-FTIR measurement for CO detection using hemoglobin.** Hemoglobin was loaded on a silicon ATR prism, and an NHase solution and *t*BuNC were separately placed in a sealed space. *t*BuNC was supplied to the NHase solution as a vapor, and the reaction was initiated by photoactivation of NHase.

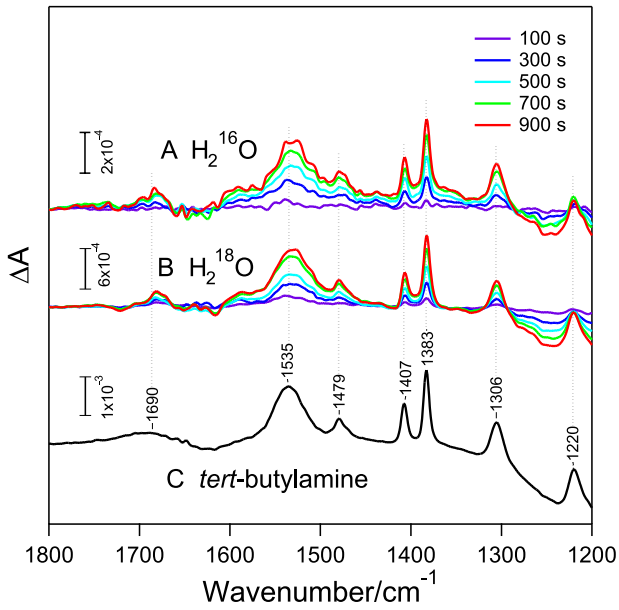

FIGURE 2. **ATR-FTIR difference spectra showing product formation by the NHase reaction with *t*BuNC.** FTIR spectra of $H_2{}^{16}O$ (*A*) and $H_2{}^{18}O$ (*B*) solutions including NHase and *t*BuNC were recorded before and 100 (*purple*), 300 (*blue*), 500 (*cyan*), 700 (*green*), and 900 (*red*) s after illumination of *Re*NHase, and difference spectra were calculated relative to before illumination values. *C*, the spectrum of *t*BuNH_2 in an aqueous solution (in a protonated *t*Bu$NH_3{}^+$ form) after subtraction of water absorption is presented for comparison.

Light-induced difference spectra were calculated by subtracting the dark spectra from each spectrum after illumination. The base-line distortion was corrected by subtracting the corresponding spectra measured in the same manner but without illumination.

For CO detection, 6 μl of hemoglobin (50 mg/ml) in 50 mM Tris-HCl, pH 7.5, was lightly dried on a silicon ATR prism, and 6 μl of the nitrosylated *Re*NHase sample (70 mg/ml) in Tris-HCl, pH 7.5, was placed beside the hemoglobin. The sample space was sealed with a CaF_2 plate, on which 0.5 μl of *t*BuNC was placed, and a greased Teflon spacer (Fig. 1). The *Re*NHase sample was photoactivated by white light illumination for 1 min. FTIR spectra with 10-s scans were recorded at 0, 20, 30, and 60 min after illumination.

Crystallization of ReNHase—Crystals of the nitrosylated *Re*NHase were grown using the vapor diffusion hanging drop method at 20 °C. Two microliters of the nitrosylated *Re*NHase (20 mg/ml protein in 50 mM Tris-HCl, pH 7.5) was mixed with an equal amount of the precipitant solution (20% polyethylene

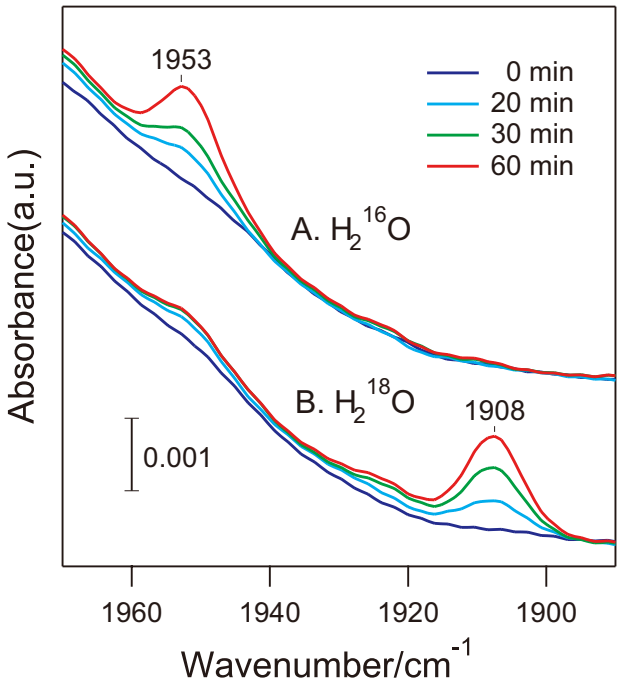

FIGURE 3. **The CO stretching region of the ATR-FTIR spectra of hemoglobin.** Hemoglobin was loaded on an Si ATR prism, and NHase in an $H_2{}^{16}O$ (*A*) or $H_2{}^{18}O$ (*B*) buffer and *t*BuNC were separately placed in a sealed space (Fig. 2). The spectra at 0 (*blue*), 20 (*cyan*), 30 (*green*), and 60 (*red*) min after photoactivation of NHase were recorded.

glycol 8000, 0.10 M Tris-HCl, pH 7.5, 0.30 M $MgCl_2$) and equilibrated against 0.40 ml of precipitant solution. Crystals with dimensions of approximately $0.4 \times 0.3 \times 0.3$ mm^3 grew within a day in the dark at 20 °C. When crystals of the nitrosylated NHase were dissolved in 50 mM Tris-HCl, pH 7.5, the enzyme solution exhibited trace amounts of methacrylonitrile hydration activity in the dark, but it had a specific activity of 7.3×10^2 units/mg after light-induced denitrosylation (10,000 l×) with a cold light illumination system (LG-PS2; Olympus, Tokyo, Japan) for 15 min.

Preparation of the ReNHase Crystals without or with tBuNC—Crystals of the nitrosylated *Re*NHase were first vapor-soaked with cryoprotectant solution (30% polyethylene glycol 8000, 0.10 M Tris-HCl, pH 7.5, 0.60 M $MgCl_2$) for 1 day by being swapped in mother liquor. They were then vapor-soaked for a day with mother liquor solution containing *t*BuNC at a final concentration of 0.10 M. After being mounted, *Re*NHases in the crystals were activated by light-induced denitrosylation (10,000 l×) with a cold light illumination system (LG-PS2; Olympus), and the reaction proceeded for 18, 120, 340, and 440 min at 20 °C. At each elapsed time, the reaction was terminated by flash cooling with N_2 gas at 95 K.

X-ray Data Collections, Structure Determinations, and Refinements—Diffraction data were collected using a Quantum 315 CCD detector (Area Detector Systems Corporation, Poway, CA) at the beamline BL-5A ($\lambda = 1.000$ Å) of the Photon Factory (Tsukuba, Japan) at 95 K. Each data set was indexed, merged, and scaled with the HKL2000 program suite (24). The

TABLE 1
Data collection and refinement statistics

	Nitrosylated NHase[a]	0 min[a,b]	18 min[a]	120 min[a]	340 min[a]	440 min[a]
Data collection						
Space group	*C2*	*C2*	*C2*	*C2*	*C2*	*C2*
Cell dimensions						
a (Å)	114.7	114.0	114.0	114.1	113.9	114.0
b (Å)	60.5	60.0	60.0	60.1	60.2	60.2
c (Å)	81.9	81.7	81.7	81.7	81.4	81.5
α, β, γ (°)	125.0	125.1	125.1	125.1	125.1	125.1
Wavelength (Å)	1.00000	1.00000	1.00000	1.00000	1.00000	1.00000
Resolution (Å)	50.0-1.30	50.0-1.48	50.0-1.48	50.0-1.39	50.0-1.59	50.0-1.49
Resolution of highest resolution shell (Å)	1.35-1.30	1.53-1.48	1.53-1.48	1.44-1.39	1.65-1.59	1.54-1.49
R_{merge}	0.051	0.035	0.038	0.038	0.036	0.042
R_{merge} of highest resolution shell	0.293	0.118	0.108	0.271	0.208	0.216
$I/\sigma I$	24.4	26.8	26.1	24.1	27.9	24.4
$I/\sigma I$ of highest resolution shell	3.49	10.5	10.8	3.71	4.04	3.97
Completeness (%)	98.8	98.3	97.0	98.0	97.3	93.8
Completeness of highest resolution shell (%)	97.2	93.6	93.1	90.2	85.3	75.9
Redundancy	3.7	2.1	2.0	1.8	1.8	1.9
Refinement						
Resolution (Å)	7.96-1.30	8.00-1.48	8.00-1.48	7.98-1.39	7.99-1.59	8.00-1.49
No. reflections	105,634	69,876	68,831	84,855	55,536	65,146
R_{work}/R_{free}	16.9/18.7	16.8/19.4	16.8/19.0	17.7/20.1	15.8/18.5	15.9/18.3
No. atoms						
Protein	3,288	3,252	3,255	3,222	3,185	3,185
Ligand/ion	4	5	5	5	12	13
Water	756	663	643	601	538	545
B-factors						
Protein	11.7	13.4	14.1	14.5	11.2	11.7
Ligand/ion	18.7	16.6	20.9	29.8	18.6	20.4
Water	28.8	28.3	29.1	20.7	27.2	28.6
Root mean square deviations						
Bond length (Å)	0.007	0.008	0.008	0.007	0.009	0.007
Bond angles (°)	1.151	1.198	1.188	1.184	1.184	1.160
Ramachandran plot						
Most favored (%)	98.5	98.0	98.2	98.5	98.2	98.2
Additionally allowed region (%)	1.5	2.0	1.8	1.5	1.8	1.8

[a] One crystal was used to collect the data of each complex.
[b] "0 min" represents nitrosylated NHase soaked with *t*BuNC.

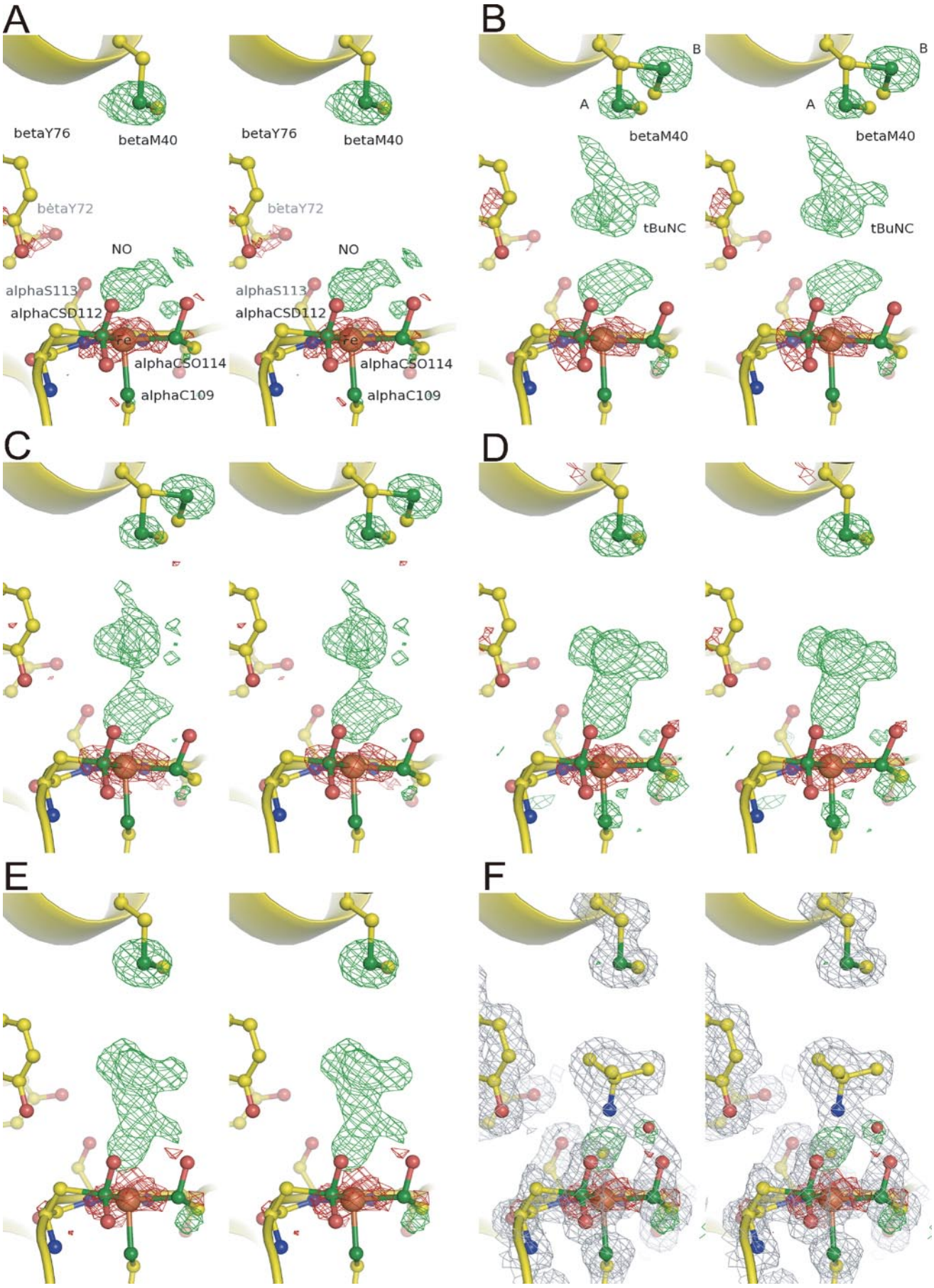
A
betaY76
betaM40
betaY72
NO
alphaS113
alphaCSD112
Fe
alphaCSO114
alphaC109
B
A
B
betaM40
tBuNC
C
D
E
F

*Re*NHase crystals belonged to the C2 space group. One heterodimer of α and β subunits populated the asymmetric unit. Molecular replacement was performed with MOLREP (25) in the CCP4 program suite (26) using the structure of the nitrosylated *Re*NHase in the $P2_12_12$ space group (Protein Data Bank code 2ahj) (7) as the initial coordinates. The obtained models were improved by iterative cycles of crystallographic refinement using REFMAC5 (27) and manual model rebuilding using Coot (28). The models were cross-validated by the SigmaA-weighted electron density maps (29) calculated with both $2mF_{obs} - DF_{calc}$ and $mF_{obs} - DF_{calc}$ coefficients. The refinements were performed using a maximum likelihood target with bulk solvent corrections. During the structure refinement, ~5% of the amplitude data were set aside to monitor the progress of refinement using the R_{free} factor. Solvent water molecules were gradually introduced if the peaks that were contoured at more than 4.0 σ in the $mF_{obs} - DF_{calc}$ electron density were in the range of a hydrogen bond. *tert*-Butyl groups of *t*BuNC were fit on the resultant difference electron density map by handling, and their coordinate data were then refined using REFMAC5 (27). All of the structural figures were generated using PyMol.

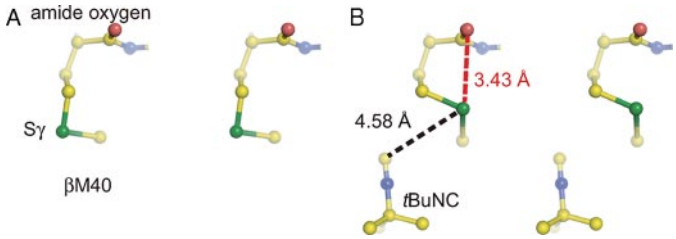

FIGURE 5. **The steric hindrance at Sγ of βMet40 caused by *t*BuNC.** The refined structure around βMet^{40} in the nitrosylated NHase without (*A*) and with (*B*) *t*BuNC. *Yellow*, *blue*, *red*, and *green spheres* represent carbon, nitrogen, oxygen, and sulfur atoms, respectively. The *black* and *red dashed lines* indicate the distances between Sγ of βMet^{40} and the isonitrile carbon and between Sγ of βMet^{40} and the amide oxygen of βMet^{40}.

TABLE 2
Selected bond lengths for the complex of nitrosylated NHase with *t*BuNC after light irradiation for 440 min

	Bond lengths
	Å
Fe-C(-NC)	2.1
C(-NC)-N(-NC)	1.4
C(-NC)-O(H_2Oa)	2.3
N(-NC)-O(H_2Oa)	1.8
O(SO)-O(H_2Oa)	1.6

RESULTS AND DISCUSSION

Identification of the Product from the Isonitrile Carbon by ATR-FTIR Measurements—To identify all products except for the amine, the reaction was monitored using ATR-FTIR. *t*BuNC was added as a vapor to nitrosylated NHase, and the enzyme was activated by light-induced denitrosylation. Several prominent positive peaks, all arising from *tert*-butylamine (*t*$BuNH_2$), increased their intensities as the reaction proceeded, whereas no signals from other origins were detected (Fig. 2). Supposing that the other product possessing a carbon atom was CO, which escaped from the solution as a gas, we attempted CO detection by trapping using hemoglobin. Hemoglobin was located on a silicon ATR crystal, and nitrosylated *Re*NHase solution and *t*BuNC were separately placed in a sealed space (Fig. 1). A CO molecule-bound hemoglobin was monitored by ATR-FTIR after light activation of *Re*NHase (Fig. 3). The CO stretching signal of CO-hemoglobin was observed at 1953 cm^{-1}, and its intensity increased with the reaction time. The CO peak appeared at a downshifted frequency of 1908 cm^{-1} when the *Re*NHase reaction was performed in an $H_2{}^{18}O$ buffer, confirming that CO was produced by the *Re*NHase-consuming water. Thus, we concluded that *Re*NHase hydrolyzed *t*BuNC to produce *t*$BuNH_2$ and CO (*t*BuNC + $H_2O \rightarrow$ *t*$BuNH_2$ + CO).

Time-resolved X-ray Crystallography of the Reaction of ReNHase with tBuNC—Crystals of nitrosylated *Re*NHase were soaked with *t*BuNC, and the reaction was started by light-induced denitrosylation at 293 K. At 18, 120, 340, and 440 min, the reaction was stopped by flash cooling at 95 K, at which point the crystal structure was determined. Details of data collection and refinement statistics are summarized in Table 1. Unfortunately, we could not collect data from the crystals that were incubated longer because those crystals were damaged. The overall structure at each elapsed time was essentially unchanged except for the pocket above the Fe^{3+} center (Fig. 4). αCys^{112}-SO_2^- (αCSD112) and αCys^{114}-SO^- (αCSO114) modifications were clearly observed in all of the structures determined.

Before soaking with *t*BuNC, an NO molecule was observed at a distance of 2.1 Å from the Fe^{3+} (Fig. 4*A*). The Fe-N(NO) distance is 0.6 Å longer than observed in the previous structure (Protein Data Bank code 2ahj) (7). In the previous structure, the NO was likely to be pushed toward Fe^{3+} by 1,4-dioxane, the co-precipitant used (7). After soaking with *t*BuNC, the electron density of *t*BuNC was clearly observed in the pocket (Fig. 4*B*) with the *tert*-butyl group facing the NO molecule coordinated to the Fe^{3+}. Because of the limited space in the hydrophobic pocket, the bulky *tert*-butyl group must face the iron in its nitrosylated state. In addition to the original conformation (conformer A), Sγ of βMet^{40} took another conformation (conformer B) with occupancies of A:B = 0.25:0.75. Movement of Sγ of βMet^{40} to conformer B is likely due to the occupation of the hydrophobic pocket by *t*BuNC. We hypothesize that conformer B is less stable because of steric hindrance between Sγ and the amide oxygen of βMet^{40} (Fig. 5).

At 18 min, electron densities of NO and *t*BuNC, especially that of the isonitrile group, were attenuated (Fig. 4*C*). Sγ of βMet^{40} remained disordered, but the occupancy of conformer A increased to 0.55. At 120 min, the NO disappeared, and a *t*BuNC molecule was coordinated to Fe^{3+} with an Fe-C(-NC)

FIGURE 4. **Structures around the non-heme Fe^{3+} center of *Re*NHase.** $F_o - F_c$ electron densities (3.0 σ contour as *green* and −3.0 σ contour as *red*) superimposed on the refined structures. NO and *t*BuNC molecules and Sγ of βMet^{40} were excluded from the calculation. *A*, nitrosylated NHase before soaking; *B*, nitrosylated NHase with *t*BuNC; *C–E*, NHase with *t*BuNC after light illumination for 18 (*C*), 120 (*D*), and 440 min (*E*). *F*, $F_o - F_c$ electron density (3.0 σ contour as *green* and −3.0 σ contour as *red*) and $2F_o - F_c$ electron density (1.0 σ contour as *gray*) superimposed on the refined structure at 440 min. *t*$BuNH_2$ was included in the calculation. *alphaCSD112* and *alphaCSO114* indicate αCys^{112}-SO_2^- and αCys^{114}-SO^-, respectively. *Yellow*, *blue*, *red*, *green*, and *brown spheres* represent carbon, nitrogen, oxygen, sulfur, and iron atoms, respectively.

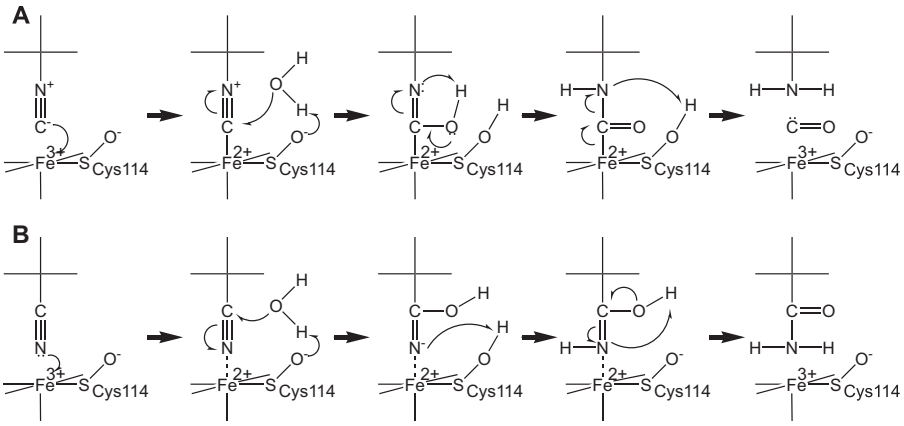

FIGURE 6. **Proposed catalytic mechanisms of NHase.** *A*, isonitrile hydrolysis. *B*, nitrile hydration.

length of 2.1 Å (Fig. 4*D*). βMet^{40} took conformer A again. The rotation of the *t*BuNC molecule could be driven by the recovery of βMet^{40} to conformer A.

The $F_o - F_c$ electron density at 340 (supplemental Fig. S1) and 440 min (Fig. 4*E*) were very similar to one another but distinct from those observed at 120 min. In both structures, the $F_o - F_c$ electron density corresponding to the *tert*-butyl group was moved ~1.0 Å away from the iron, and an extra electron density was observed near the isonitrile carbon as well as the sulfenate oxygen of αCys^{114}. When the products, *t*BuNH$_2$ and CO, were included in the calculation of the electron density at 440 min, the refined model of *t*BuNH$_2$ was well fit on the $2F_o - F_c$ electron density, but that of CO was not (supplemental Fig. S2). In addition, two positive electron densities were observed near the CO molecule in the $F_o - F_c$ electron density. Alternatively, we calculated the electron density at 440 min by assuming the presence of only *t*BuNH$_2$. As shown in Fig. 4*F*, *t*BuNH$_2$ was well fit on the $2F_o - F_c$ electron density, and two positive electron densities were observed above the iron ion and near Oδ of the sulfenate group, in the $F_o - F_c$ electron density. We assigned the positive densities as the carbon of the isonitrile group and the solvent water molecule (named as H$_2$Oa), respectively (Fig. 4*F*). All distances of Fe-C(-NC), C(-NC)-N(-NC), C(-NC)-O(H$_2$Oa), N(-NC)-O(H$_2$Oa), and O(H$_2$Oa)-O(-SO) converged at less than 2.2 Å (Table 2). The O(H$_2$Oa)-O(-SO) distance cannot be explained. These atoms may be disordered because the occupancies of H$_2$Oa and Oδ of αCys^{114}-SO$^-$ converged on 0.50. Interestingly, a positive difference density was observed below Sγ of αCys^{114}-SO$^-$ in the $2F_o - F_c$ electron density map after coordination of *t*BuNC (Fig. 4, *D–F*). The distance between the density and Sγ of αCys^{114}-SO$^-$ is 1.4 Å, and the angle Oδ(αCys^{114}-SO$^-$) − Sγ(αCys^{114}-SO$^-$) − the density was 133°. The positive density may represent an alternative position of Oδ of αCys^{114}-SO$^-$.

Proposed Catalytic Mechanisms of NHase—Based on the results, we propose the following catalytic mechanism: the *t*BuNC substrate binds the metal directly, and then a water molecule, activated by Oδ of αCys^{114}-SO$^-$, makes a nucleophilic attack on the isonitrile carbon to produce *t*BuNH$_2$ and CO (Fig. 6*A*). Considering the similarity between isonitriles and nitriles, nitrile hydration is likely to proceed in a similar manner (Fig. 6*B*). When a nitrile coordinates to the metal, the nitrile carbon is attacked by a water molecule, activated by Oδ of αCys^{114}-SO$^-$. The low k_{cat} value for isonitrile may be due to limited accessibility of the activated water molecule because of steric hindrance by Oδ of αCys^{114}-SO$^-$. Nitrile coordination to the Fe^{3+} was suggested by electron spin resonance measurements (30). Involvement of αCys^{114}-SO$^-$ in the catalytic reaction had been suggested by our previous studies using the inhibitor, 2-cyano-2-propyl hydroperoxide (13), specifically oxidizing αCys^{114}-SO$^-$ to Cys-SO$_2^-$, and the site-directed mutant NHases (31). Yano *et al.* (32) have extensively studied the N$_2$S$_2$(*t*BuNC)$_2$-type Co^{3+} model complexes with different sulfur oxidation states and concluded that sulfur oxidations promoted the Lewis acidity of the Co^{3+} center and that only the sulfenyl oxygen exhibited a nucleophilic character. Theoretical calculation studies have indicated that Oδ of αCys^{114}-SO$^-$ could be a catalytic base when nitrile coordination was assumed (19). These antecedent studies support the mechanism of the substrate coordinated to the iron being attacked by water activated by αCys^{114}-SO$^-$. Recently, involvement of the Ser ligand (αSer^{112}; corresponding to αSer^{113} of *Re*NHase) and of the vicinal Tyr and Trp residues (βTyr^{68} and βTrp^{72}; corresponding to βTyr^{72} and βTyr^{76} of *Re*NHase) in the catalytic mechanism was suggested by temperature- and pH-dependent kinetic studies of the Co-type NHase from *Pseudonocardia thermophila* JCM 3095 (33). However, the corresponding residues of *Re*NHase were unchanged during our investigations (Fig. 4). Our findings represent the first structural evidence of reaction intermediates in NHase catalysis. The present results demonstrate a reaction mechanism in which the sulfenate group of αCys^{114}-SO$^-$ plays a key role in the catalysis. Cysteine oxidation has been found to play important roles in various proteins (34). The present work reveals a novel role of cysteine sulfenic acid as a catalytic base.

Acknowledgments—We are grateful to beamline assistants of the Photon Factory for data collection at beamline BL-5A. We thank Drs. K. Noguchi and A. Ohtaki (Tokyo University of Agriculture and Technology), Prof. N. Kamiya (Osaka City University), and Dr. M. Nojiri (Osaka University) for useful advice and discussion on the structural determination and analyses of the intermediate structure of NHase. We also thank Prof. K. Nagasawa and Mr. M. Tera (Tokyo University of Agriculture and Technology) and Prof. T. Ozawa (Nagoya Institute of Technology) for fruitful discussion on the catalytic mechanism.

REFERENCES

1. Kobayashi, M., and Shimizu, S. (1998) *Nat. Biotechnol.* **16,** 733–736
2. Endo, I., Nojiri, M., Tsujimura, M., Nakasako, M., Nagashima, S., Yohda, M., and Odaka, M. (2001) *J. Inorg. Biochem.* **83**, 247–253
3. Noguchi, T., Hoshino, M., Tsujimura, M., Odaka, M., Inoue, Y., and Endo, I. (1996) *Biochemistry* **35,** 16777–16781

4. Odaka, M., Fujii, K., Hoshino, M., Noguchi, T., Tsujimura, M., Nagashima, S., Yohda, M., Nagamune, T., Inoue, Y., and Endo, I. (1997) *J. Am. Chem. Soc.* **119,** 3785–3791
5. Bonnet, D., Artaud, I., Moali, C., Petre, D., and Mansuy, D. (1997) *FEBS Lett.* **409,** 216–220
6. Huang, W., Jia, J., Cummings, J., Nelson, M., Schneider, G., and Lindqvist, Y. (1997) *Structure* **5,** 691–699
7. Nagashima, S., Nakasako, M., Dohmae, N., Tsujimura, M., Takio, K., Odaka, M., Yohda, M., Kamiya, N., and Endo, I. (1998) *Nat. Struct. Biol.* **5,** 347–351
8. Miyanaga, A., Fushinobu, S., Ito, K., and Wakagi, T. (2001) *Biochem. Biophys. Res. Commun.* **288,** 1169–1174
9. Hourai, S., Miki, M., Takashima, Y., Mitsuda, S., and Yanagi, K. (2003) *Biochem. Biophys. Res. Commun.* **312,** 340–345
10. Arakawa, T., Kawano, Y., Kataoka, S., Katayama, Y., Kamiya, N., Yohda, M., and Odaka, M. (2007) *J. Mol. Biol.* **366,** 1497–1509
11. Noguchi, T., Nojiri, M., Takei, K., Odaka, M., and Kamiya, N. (2003) *Biochemistry* **42,** 11642–11650
12. Murakami, T., Nojiri, M., Nakayama, H., Odaka, M., Yohda, M., Dohmae, N., Takio, K., Nagamune, T., and Endo, I. (2000) *Protein Sci.* **9,** 1024–1030
13. Tsujimura, M., Odaka, M., Nakayama, H., Dohmae, N., Koshino, H., Asami, T., Hoshino, M., Takio, K., Yoshida, S., Maeda, M., and Endo, I. (2003) *J. Am. Chem. Soc.* **125,** 11532–11538
14. Shearer, J., Kung, I. Y., Lovell, S., Kaminsky, W., and Kovacs, J. A. (2001) *J. Am. Chem. Soc.* **123,** 463–468
15. Lugo-Mas, P., Dey, A., Xu, L. K., Davin, S. D., Benedict, J., Kaminsky, W., Hodgson, K. O., Hedman, B., Solomon, E. I., and Kovacs, J. A. (2006) *J. Am. Chem., Soc.* **128,** 11211–11221
16. Noverson, J. C., Olmstead, M. M., and Mascharak, P. K. (1999) *J. Am. Chem. Soc.* **121,** 3553–3554
17. Tyler, L. A., Noverson, J. C., Olmstead, M. M., and Mascharak, P. K. (2003) *Inorg. Chem.* **42,** 5751–5761
18. Heinrich, L., Mary-Verla, A., Li, Y., Vassermann, J., and Chottard, J. C. (2001) *Eur. J. Inorg. Chem.* **9,** 2203–2206
19. Hopmann, K. H., Guo, J. D., and Himo, F. (2007) *Inorg. Chem.* **46,** 4850–4856
20. Hopmann, K. H., and Himo, F. (2008) *Eur. J. Inorg. Chem.*, **2008,** 1406–1412
21. Kubiak, K., and Nowak, W. (2008) *Biophys. J. (2008)* **94,** 3824–3838
22. Taniguchi, K., Murata, K., Murakami, Y., Takahashi, S., Nakamura, T., Hashimoto, K., Koshino, K., Dohmae, N., Yohda, M., Hirose, T., Maeda, M., and Odaka, M. (2008) *J. Bioeng. Biosci.* **106,** 174–179
23. Tsujimura, M., Odaka, M., Nagashima, S., Yohda, M., and Endo, I. (1996) *J. Biochem.* (*Tokyo*) **119,** 407–413
24. Otowinowski, Z., and Minor, W. (1997) *Methods Enzymol.* **276,** 307–326
25. Vagin, A., and Teplyakov, A. (1997) *J. Appl. Crystallogr.* **30,** 1022–1024
26. CCP4 (Collaborative Computational Project, Number 4) (1994) *Acta Crystallogr. Sect. D Biol. Crystallogr.* **50,** 760–763
27. Murshudov, G. N., Vargin, A. A., and Dodson, E. J. (1997) *Acta Crystallogr. Sect. D Biol. Crystallogr.* **53,** 240–255
28. Emsley, P., and Cowtan, K. (2004) *Acta Crystallogr. Sect. D Biol. Crystallogr.* **60,** 2126–2132
29. Read, R. J. (1986) *Acta Crystallogr. Sect. A* **42,** 140–149
30. Sugiura, Y., Kuwahara, J., Nagasawa, T., and Yamada, H. (1987) *J. Am. Chem. Soc.* **109,** 5848–5850
31. Takarada, H., Kawano, Y., Hashimoto, K., Nakayama, H., Ueda, S., Yohda, M., Kamiya, N., Dohmae, N., Maeda, M., and Odaka, M. (2006) *Biosci. Biotechnol. Biochem.* **70,** 881–889
32. Yano, T., Wasada-Tsutsui, Y., Arii, H., Yamaguchi, S., Funahashi, Y., Ozawa, T., and Masuda, H. (2007) *Inorg. Chem.* **46,** 10345–10353
33. Mitra, S., and Holz, R. C. (2007) *J. Biol. Chem.* **282,** 7397–7404
34. Claiborne, A., Mallett, T. C., Yeh, J. I., Luba, J., and Parsonage, D. (2001) *Adv. Protein Chem.* **58,** 215–276